Functionality assessment of road network combining flood roadworthiness and graph topology

He, Ke; Pregnolato, Maria; Carhart, Neil; Neal, Jeffrey; De Risi, Raffaele

DOI
10.1016/j.trd.2024.104354

Publication date
2024

Document Version
Final published version

Published in
Transportation Research Part D: Transport and Environment

Transportation Research Part D xxx (xxxx) xxx

Contents lists available at ScienceDirect

Transportation Research Part D

journal homepage: www.elsevier.com/locate/trd

Functionality assessment of road network combining flood roadworthiness and graph topology

Ke He [a], Maria Pregnolato [a,b], Neil Carhart [a], Jeffrey Neal [c], Raffaele De Risi [a,*]

[a] School of Civil, Aerospace and Design Engineering, University of Bristol, Bristol BS8 1TR, UK
[b] Dept. of Hydraulic Engineering, Delft Univ. of Technology, Delft 2628 CN, Netherlands
[c] School of Geographical Sciences, University of Bristol, Bristol BS8 1SS, UK

ARTICLE INFO

Keywords:
Hazard intensity measures
Safety and severity factors
Link classification
OpenStreetMap
NetworkX
Network performance

ABSTRACT

Flood hazards can affect road networks by closing roads, extending travel distances and lengthening travel times. This paper innovatively integrates flood hazard, road network topology and vehicle vulnerability via a severity factor to assess the accessibility of exposed links and the performance of the whole network. The overall network functionality loss under different flood return periods is assessed by evaluating the functionality of each network link for cars and SUVs. The most vulnerable links are identified and used to assess the performance of the entire network using topology-based metrics such as average shortest paths and isochrones. The case study of Bristol (UK) is investigated. It is demonstrated that network status is a function of vehicle typology, with SUVs exhibiting naturally stronger resistance to flood than cars. This finding can support preparedness strategies of road networks in the face of future flood events.

1. Introduction

Road networks are vital for societal development, economic growth and human activities (Evans et al., 2020). They function as the arteries of cities and nations, connecting different geographical areas. In the last two decades, the increasing frequency of extreme weather due to climate change has severely affected many infrastructures, making road networks non-functional and threatening human life and economic growth (Abdulla et al., 2020; Wardhana & Hadipriono, 2003). For example, from 1989 to 2000, 53 % of all reported bridge collapses in the United States were attributed to water-related disasters, with 32.8 % of these directly linked to flooding events (Wardhana & Hadipriono, 2003). In 2007, the UK experienced severe rainfall and floods that significantly impacted the road network, resulting in an estimated £60 million in damages (Argyroudis et al., 2020). In 2009, the UK faced a severe flooding event in Cumbria that led to the collapse of more than 20 bridges, one fatality and restoration costs of hundred millions of GBP (Cumbria County Council, 2010). Pluvial flash floods caused widespread transportation disruption and 79 deaths due to inundated roads in July 2012 in Beijing, China (Yin et al., 2014). Following the inundation of road networks, travellers must either cancel their journey or find alternative paths, increasing both travel distance and time, exacerbating traffic congestion and causing a drastic reduction of vehicular speeds within the network (Pregnolato et al., 2017; Pyatkova et al., 2018; Wang, 2018). Nelson et al. (2021) demonstrated that a simple 10-year return period inundation scenario in Beira, Mozambique, may lead to an increased travel time of 103 % for the local transportation network. In 2023, the Chinese Hebei province was struck by Typhoon Doksuri, leading to severe flooding and posing a significant threat to the affected regions. The associated floods left many residents stranded, destroyed bridges and highways and

* Corresponding author.
E-mail address: raffaele.derisi@bristol.ac.uk (R. De Risi).

https://doi.org/10.1016/j.trd.2024.104354
Received 28 November 2023; Received in revised form 13 June 2024; Accepted 5 August 2024

ultimately caused 30 fatalities (McCarthy & Magramo, 2023). All these events show that floods pose a threat to human lives, disrupt travel, and lead to massive economic losses. Therefore, mitigating the impact of floods on road networks is a current focal point for researchers.

Many studies have explored these issues in recent years, often proposing methods for quantifying system resilience. Bruneau et al. (2003) defined infrastructure resilience as the infrastructure's capacity to resist damage and maintain functionality during and after a disaster. Numerous researchers have studied flood hazard impacts on road networks via multiple approaches. One approach involves the static analysis of flood hazards on roads, where the functionality loss of the road network is assessed by simply overlaying hazard maps with the road network without considering traffic features (Jalayer et al., 2014; De Risi et al., 2015; Kalantari et al., 2017; De Risi et al., 2018; Casali & Heinimann, 2019; Zhang & Alipour, 2019; De Risi et al., 2020; He et al., 2023). In the context of road network graph-based modelling, the prevailing approach involves representing roads as links and intersections as nodes, using global topological indicators such as the average node degree or the average shortest path to assess the performance of the network (Alabbad et al., 2021; Boeing, 2017a; Casali and Heinimann, 2019; Cimellaro et al., 2010; Evans et al., 2020; Gauthier et al., 2018; Karduni et al., 2016; Merschman et al., 2020; Nelson et al., 2019; Ogie et al., 2018; Pregnolato et al., 2016; Zhang et al., 2019; He et al., 2023; Henry et al., 2021). As the main road network topological data source, OpenStreetMap is often used as it provides comprehensive geospatial features through an open-source database (Costa Fonte et al., 2017).

An alternative approach focuses on the dynamic nature of both flooding and road networks, involving the evaluation of changes in traffic flow, travel times, and travel distances within the road network (Hooper et al., 2012; Balijepalli & Oppong, 2014; Do & Jung, 2018; El Rashidy & Grant-Muller, 2019; Shahdani et al., 2022). However, due to the significant uncertainty in traffic within the road network, it remains challenging to accurately model the evolving traffic dynamics resulting from road closures due to flooding. While agent-based approaches like SUMO and MATSim can dynamically simulate traffic flow variations in networks (Barthélemy & Carletti, 2017; Lopez et al., 2018; Muhammad et al., 2024), the driver behaviour after the flooding is still uncertain (e.g. cognitive dissonance). As a result, many studies have opted to focus on the variations in traffic flow and travel times along specific roads within the network as a means to depict the effects of flood hazards on the road network (Yin et al., 2016; Pregnolato et al., 2017; Otković et al., 2020; Shahdani et al., 2022).

When the road network is affected by flood hazards, the most vulnerable components within the network are the vehicles (Arrighi et al., 2015). It is paramount to assess whether vehicles are capable of transit over a specific inundated link; this vehicle property is here defined as flood roadworthiness. The roadworthiness includes limitations due to the vehicle design (e.g., the heights of air inlets), as well as vehicle stability (e.g., aquaplaning, floating, sliding, and tipping) (Pregnolato et al., 2017). The two primary intensity measures of flood hazards affecting vehicle stability are flood depth and flow velocity (Bocanegra & Francés, 2021). The impact of flood depth on vehicles consists of reducing the maximum travel speed to ensure their safe passage through inundated roads. Both discrete (Shahdani et al., 2022) and continuous (Pregnolato et al., 2016; Pregnolato et al., 2017; Choo et al., 2020) methods exploring the relationship between vehicle speed and flood depth reveal that vehicles cannot travel under a flood depth of 0.3 m.

In a recent study, three primary methods, namely depth-centric, probabilistic and stability-centric, are employed to assess the feasibility of vehicles passing through flooded roads (Panakkal et al., 2023). The flood stability is mainly governed by the flood flow velocity. The impact of flood flow velocity on vehicle stability has primarily been assessed in the literature through experimental methods to determine critical thresholds. This involved subjecting scaled-down vehicle models to various incipient flood directions in order to assess the stability of different vehicle types under flooding (Shu et al., 2011; Xia et al., 2011b; Teo et al., 2012; Toda et al., 2013; Xia et al., 2014; Kramer et al., 2016; Xia et al., 2016).

Experimental findings have demonstrated that critical instability occurs when incipient flood flow is perpendicular to the lateral sides of the vehicle (Wang et al., 2021). The maximum flood flow velocity the vehicle can withstand is also known as critical flood velocity (Xia et al., 2011a). Moreover, it has been observed that the critical flood velocity decreases with increasing floodwater depth (Xia et al., 2011a; Martínez-Gomariz et al., 2017; Wang et al., 2021; Lazzarin et al., 2022). However, there is currently a lack of research that integrates the effects of flood depth and flood velocity on vehicles. Many studies have predominantly focused on binary conditions of road functionality (i.e., accessible, not accessible). Although some researchers have studied how natural hazards (e.g., side-wind) impact vehicle stability (Kim et al., 2020; Kim et al., 2022), the state-of-the-art in flood hazards still lacks granularity in the description of the link conditions during floods, such as when and how much vehicles must reduce their travel speed based on different severity levels (Kim et al., 2016).

The most common metrics for evaluating the overall functionality of a whole transport network are the graph-based topological features of average node degree, average clustering coefficient and average shortest path (Cimellaro et al., 2011; Mukherjee, 2012; Boeing, 2017b; Zhang & Alipour, 2019; He et al., 2023). These metrics allow a rapid assessment of the impact of the closure of a specific link on the overall road network. Furthermore, Panakkal et al. (2023) also demonstrated that it is important to compute and visualise the reduced accessibility of critical amenities (e.g., hospitals) in areas affected by road closures due to floods. This type of computation supports pre-emptive preparedness and planning of emergency vehicle access in post-flood scenarios. However, following the binary classification defined above, the overall road network functionality assessment is limited to situations where roads have become entirely non-functional due to flood hazards. Current literature does not account for cases where roads, despite being flooded, still allow vehicular passage during flooding events.

Building upon the literature and its identified gaps, this study proposes a deterministic framework for assessing the overall functionality losses of road networks during flood events. Specifically, an innovative approach is proposed, integrating flood depth and velocity with vehicle characteristics and network topological features. First, a flood severity factor is proposed and mapped onto the road network. The assessment of each link functionality primarily relies on the road flood roadworthiness, encompassing variations in road accessibility for different vehicle types. Then, the overall functional loss of the road network is quantified using graph-based

methodologies utilising OSMnx (OpenStreetMap-NetworkX). Additionally, this study proposes time-based isochrones to assess the reduction in the reachable service range of critical amenities (e.g., hospitals) within the road network following a flood event. The findings from this research can inform the formulation of effective strategies to mitigate flood risk impacts on the road network and optimise vehicle travelling paths, ensuring better preparedness and resilience in the face of flooding.

This paper is organised into six sections. After the introduction, Section 2 describes the research methodology employed for data collection, severity classification, and the functionality loss assessment of the road network. In Section 3, a case study is presented, focusing on the functionality loss of the Bristol, UK, road network for various types of vehicles, utilising flood hazard data from the literature. Section 4 employs a mapping approach to analyse the distribution of road network severity and assess the functionality loss for different types of vehicles. Building upon the analysis results, Section 5 elucidates the significance of this study for future work while also outlining the limitations that still exist within this research. Finally, in Section 6, a summary is provided, and conclusions are drawn.

2. Methodology

The research methodology is divided into three main parts: (i) data acquisition involving flood hazard, vehicle vulnerability, and road network exposures, (ii) severity analysis of the road network during flood inundation, and (iii) loss quantification of the road network functionality. Fig. 1 shows the methodology flowchart where the three main parts are detailed, and the connections are explicitly depicted. In the following sections, all the aspects are described in detail.

2.1. Data acquisition

In assessing the functionality of a road network under flood hazard, necessary data includes flood hazard, vehicle typology, and network features. Flood hazard is usually represented by maps of flood depth and inundation flow velocity for multiple return periods (T_R). These maps are obtained by implementing hydrological/hydraulic routines (Bates et al., 2023). Road networks are usually represented using links and nodes within a Geographical Information System (GIS). Ideally, governmental bodies such as municipalities or councils should provide road information (containing road type, travelling speed, number of lanes, etc.). However, in absence of such certified data, open-source data can be used, such as those available by OpenStreetMap (Costa Fonte et al., 2017). Finally, knowing the type of vehicle that can access the road network is important. Vehicles will have different vulnerabilities to flooding depending on their features (e.g., weight, wheel size). Vulnerability functions for the different vehicles are generally available in the literature. In the absence of these models, either numerical or experimental tests can be used. The vulnerability is usually presented as the critical velocity and depth of a water flow that leads to vehicle instability (e.g., sliding, overturning, and floating).

2.2. Severity analysis

2.2.1. The link severity factor

In conventional reliability approaches, the status of a component within a system is assessed by calculating a safety factor consisting of the ratio between the capacity of the component and the demand to which it is subjected (Der Kiureghian, 2022). With respect to conventional risk terminology, the demand is the hazard level obtained from the flood hazard assessment; the capacity is a measure of the vulnerability of the vehicles obtained from the critical flood level. Each link can be assessed by comparing the flood intensity measures (IMs) computed as the ratio between the ultimate capacity and the expected demand. This can be represented as a Severity Factor, which is the reciprocal of the safety factor, and defined as:

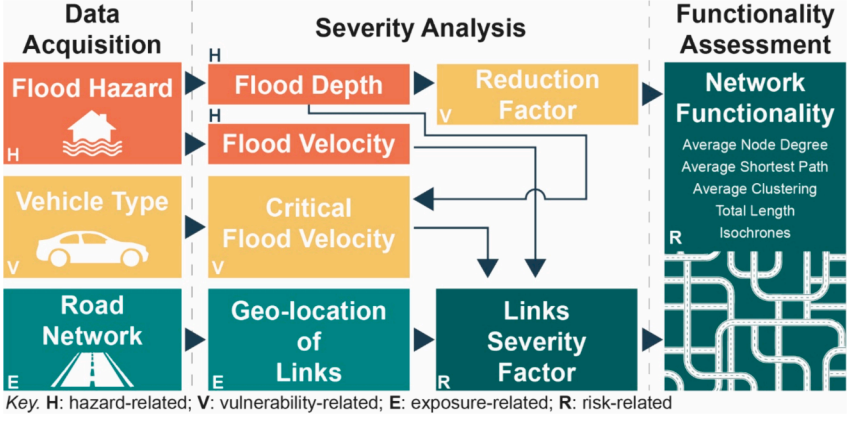

Fig. 1. Methodological flowchart of assessing functionality losses in flood disasters.

$$Sf = Severity\ factor = \frac{1}{Safety\ factor} = \frac{Demand}{Capacity} = \frac{Flood\ IM}{Critical\ flood\ IM} \tag{1}$$

The Severity factor is used herein to define the flood roadworthiness; specifically, if a link for a specific vehicle has an *Sf* larger than 1, then the link is not accessible and must not be used in case of flood. If *Sf* is lower than 1, the link is accessible; however, a classification may still be considered to suggest different levels of precaution.

2.2.2. The capacity

In Equation (1), the capacity is expressed as flood intensity measures. Specifically, it provides the IM (or the IMs) leading a vehicle to overturn or move on the road. Some models from the literature (Xia et al., 2011a; Wang et al., 2021) suggested that vehicle vulnerability can be expressed in terms of flood velocity (u) and depends on the relative direction between vehicle direction and flow velocity, vehicle dimensions, tyre properties, road surface friction, and by the flood depth (h_f) as the buoyance effect can magnify vehicle instability. These studies (Xia et al., 2011a; Wang et al., 2021) considered two distinct vehicle typologies: SUVs and cars. The critical flood velocity for flow-parallel ($\|$) and flow-perpendicular ($\perp$) directions are derived as follows:

$$u_{C,\|} = \alpha_{\|}\left(h_f/h_c\right)^{\beta_{\|}}\sqrt{2gl_c\left(\frac{\rho_c h_c}{\rho_f h_f} - R_f\right)} \tag{2}$$

$$u_{C,\perp} = \alpha_{\perp}\left(h_f/h_c\right)^{\beta_{\perp}}\sqrt{2gb_c\left(\frac{\rho_c h_c}{\rho_f h_f} - R_f\right)} \tag{3}$$

where u_C represents the critical flood velocity of vehicle instability; α and β are parameters associated with vehicle features and the road surface; h_f is the flood depth; ρ_f is the floodwater density; g is the acceleration of gravity (~9.8 m/s^2); b_c, l_c, h_c, and ρ_c, represent vehicle characteristics, namely width, height, and average density, which define the dimensions and mass distribution of the vehicle; $R_f = h_c\rho_c/\left(h_k\rho_f\right)$, where h_k is the flood depth which causes the vehicle to start floating (Xia et al., 2014; Dong et al., 2022). All the abovementioned parameters are listed in Table 1. In this study, the parameters α and β for calculating the critical flood velocity of vehicles were obtained from previous experimental studies (Xia et al., 2011a; Wang et al., 2021). Given the modular nature of the methodology, if more advanced models become available (e.g. accounting for other road features or new vehicle types), these can be seamlessly integrated like alternative modules. The vulnerability models are available only for cars and SUVs. However, if models for different vehicle typologies will be available in the future, these can be easily implemented in the framework, given the modularity of the proposed methodology.

When more than one capacity value is involved, the Severity Factor presented in Equation (1) becomes:

$$Sf = max\left\{\frac{|u| + |v|}{u_{C,\|}}, \frac{|u|}{u_{C,\perp}}\right\} \tag{4}$$

It is worth noting that, for the parallel direction, the travelling velocity of the vehicle (v) should also be considered. However, this vehicle velocity is not the maximum allowed on each link, but it is the reduced velocity compatible with the flood depth; this is explained in Section 2.2.3.

2.2.3. The vehicle velocity reduction factor

When floods submerge a road network, vehicles reduce travel velocity (v) to ensure safety. This aspect can be considered in the definition of the Severity Factor presented in Equation (4). In this study, a nonlinear relationship is employed to characterise the velocity reduction factor, which is a function of the flood depth and is equal to the ratio between the actual (v) and the maximum possible (v_{max}) vehicular velocity (Choo et al., 2020):

$$v = v_{max}e^{-9h_f} \tag{5}$$

It is worth noting that when using Equation (5) in Equation (4), the flood-parallel mechanism is the most relevant for maximum travelling speeds allowed in an urban context for flood depth lower than 30 cm. The perpendicular mechanism is dominant for flood depths over 30 cm, as also shown by Wang et al. (2021).

Table 1
Parameters for critical flood velocity both for SUVs and cars (Wang et al., 2021).

Vehicle		Parameters								
		α	β	h_c(m)	g(m/s^2)	l_c(m)	ρ_c(kg/m^3)	ρ_f(kg/m^3)	R_f	h_k(m)
SUV	$\|$	0.438	−0.219	1.737	9.8	5.089	203	1000	0.551	0.67
car	$\|$	0.212	−0.562	1.48	9.8	4.945	170.44	1000	0.65	0.45
SUV	$\perp$	0.367	−0.451	1.737	9.8	1.983	203	1000	0.551	0.67
car	$\perp$	0.492	−0.344	1.48	9.8	1.845	170.44	1000	0.65	0.45

2.2.4. Severity classification

It is possible to create a severity classification based on the values of the Severity Factor for each link and each vehicle typology (Fig. 2). According to Wang et al. (2021), six severity levels are defined based on the Severity Factor: zero inundation (Safe), (*Sf* smaller than 0.005), Low (*Sf* between 0.005 and 0.25), Low-Medium (*Sf* between 0.25 and 0.5), Medium (*Sf* between 0.5 and 0.75), Medium-High (*Sf* between 0.75 and 1), and High (*Sf* larger than 1).

A "High" severity classification signifies that the specific link is non-functional for vehicle traffic, thus considered closed and removed from the road network modelling. Vehicles are expected to adjust their driving speeds for roads classified under other severity levels according to the respective severity classification. Based on the literature (Pregnolato et al., 2016; Choo et al., 2020; Shahdani et al., 2022), this procedure represents an established approach for making informed choices regarding vehicle safety when driving through flooded roads. For the vehicles classified with lower Severity Factors, the velocity ensuring the safe passage of vehicles for the specific link can be computed according to Equations (5).

2.3. Functionality assessment

The road network can be modelled as a graph G = (V, E), where V is the set of nodes representing intersections and E is the edges representing roads within road networks. The functionality assessment of the road network uses a graph-based approach; in particular, this study employs network metrics of average node degree and average shortest path metrics (Zhang & Alipour, 2019) alongside network average clustering and aggregate road length. The definitions and equations for the used metrics are presented in Table 2. These metrics are herein computed using the NetworkX package for network analysis (NetworkX, 2022).

The status of the network can also be assessed by studying time-based isochrone maps, alternatively known as travel time maps. These maps illustrate all reachable destinations within specified constraints for a designated mode of transportation (Bainbridge, 2021). Time-based isochrones visually represent road network transportation efficiency (Coles et al., 2017; Green et al., 2017; Śleszyński et al., 2023). Thus, time-based isochrone maps based on vehicle travel can depict road network transportation efficiency changes when influenced by flood hazards. When considering critical amenities within urban areas (e.g. hospitals) as the origin points for vehicles, isochrones determine reachable areas within defined time constraints and can provide insights into the impact of road network disruptions on emergency services.

For the different hazard maps, it is possible to assess the severity levels of all the links in the network; this information can be used to compute the functionality of the network with the measures presented above. Specifically, links are simply removed from the network for "High" severity cases as they are not usable, and the network performance is re-assessed using the measures presented above. For the case of link classification with a lower safety factor, the increased travel time is assessed using the reduced vehicle velocity, as explained in Section 2.2.4. Then, the network performance is re-assessed and compared with the one computed without disruptions.

3. Case study and data resources

This study selected the city of Bristol (UK) as a case study (Fig. 3). The river Avon flows hrough the city centre, and the river Frome flows from the city centre to the North of Bristol. Bristol is a flood-prone area whose network has been repeatedly flooded (ARUP, 2020).

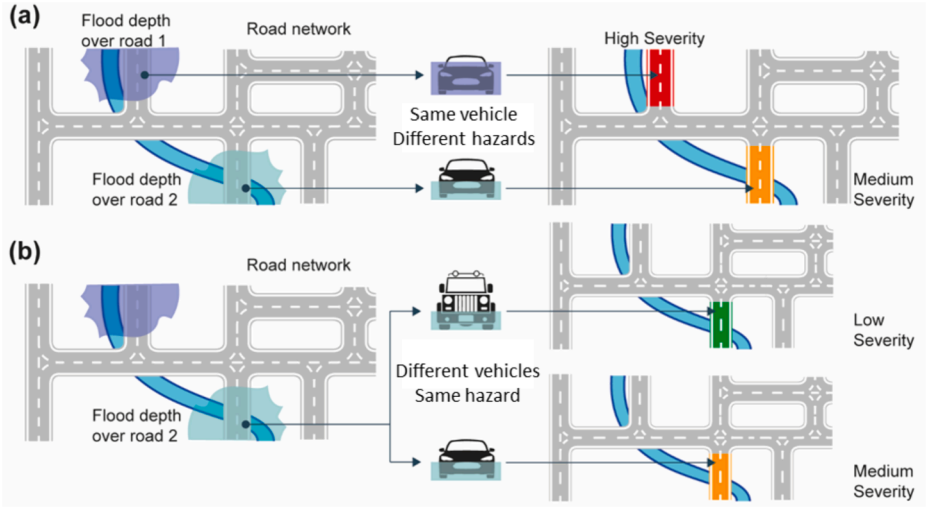

Fig. 2. Schematic representation of the road severity classification; (a) road severity classification for the same vehicle at different hazards; (b) road severity classification for different vehicles under the same hazard.

Table 2
Entire Road network functionality measures.

Measures	Definitions	Equations	Notations
Average node degree	The average number of edges connected to each node in the graph, serving as a measure of connectivity within the network.	$d_{ave} = \frac{1}{N}\sum_{j=1}^{N}\left(d_j^{in} + d_j^{out}\right)$ (7)	d_{ave}: average node degree N: number of nodes in the graph j: single node in the graph d_j^{in}: number of incoming links to node j d_j^{out}: number of outcoming links from node j
Average clustering	A measure of how well-connected and locally clustered the network is. It provides insights into the degree to which roads in a network tend to form clusters or local neighbourhoods.	$C_{ave} = \frac{1}{N}\sum\frac{2T_j}{d_j \times (d_j - 1)}$ (8)	C_{ave}: average clustering N: number of nodes in the graph d_j: degree of node j T_j: number of triangles centred at node j
Average shortest path	Overall connectivity and efficiency of information flow within the network. It can be utilised to analyse network robustness, navigation efficiency, and network optimisation strategies.	$P_{ave} = \sum_{\substack{s,t\in V \\ s\neq t}}\frac{d(s,t)}{N(N-1)}$ (9)	P_{ave}: average shortest path N: number of nodes in the graph s, t: nodes in the graph $d(s,t)$: the shortest distance from node s to node t
Total length	The overall length of operational roads in the network.	$Total\ length = \sum_{i\in E} length\ of\ fucntional\ i$ (10)	i: single edge in the graph

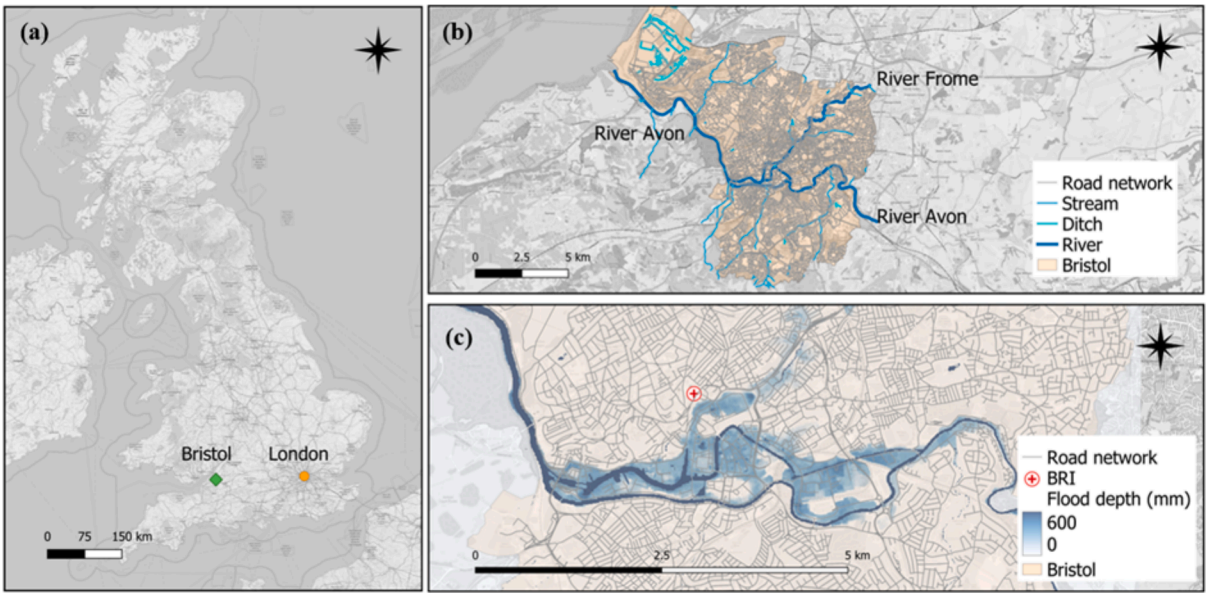

Fig. 3. Map of Bristol; (a) the location of Bristol in UK; (b) water body and road network of Bristol; (c) flood hazard map example (200-year flood return period) and Bristol Royal Infirmary (BRI) location.

The flood hazard maps used in this study have a resolution of 10 m and were provided by Fathom, a company for flood modelling (Fathom, 2023). This study does not study the sensitivity to the flood maps resolution; however, a 10 m resolution aligns well with the road's transversal width and, therefore, is deemed even more appropriate for the longitudinal extensions of the road links. However, a sensitivity analysis on the resolution of the flood hazard is desirable, if possible. For the case study at hand, the model has been validated by Bates et al. (2023).

Flood hazard maps have been computed using the LISFLOOD-FP 2D hydrodynamic model starting from a LIDAR-based digital terrain model (DTM) provided by the Environment Agency of England (Bates et al., 2023). A digital terrain model (DTM) constitutes a continuous representation of surface topography and is often employed for generating topographic maps (Podobnikar, 2009). To

reduce the computation effort, vegetation and building components were excluded from the DTM (Hawker et al., 2022). Flood depth data corresponding to ten return periods (T_R) has been used, namely of 5-, 10-, 20-, 50-, 75-, 100-, 200-, 250-, 500-, and 1000-year. The flood maps employed in this study encompass both fluvial and pluvial flooding, while drainage systems were not modelled. However, rainfall volumes are adjusted to reflect the drainage network's protection standard. Flood depth data for each flood return period is static rather than dynamic; a conservative approach is used (i.e., worst-case scenario) by considering the maximum inundation across time.

Bristol's spatial scale permits the assumption of a constant return period in space for flood events., This assumption becomes untenable on larger scales, necessitating the adoption of a stochastic model to consider multiple event scenarios (e.g. Bates et al., 2023). It is important to emphasise that flow velocity may not be available, and only flood depth is provided. The reason is that flood

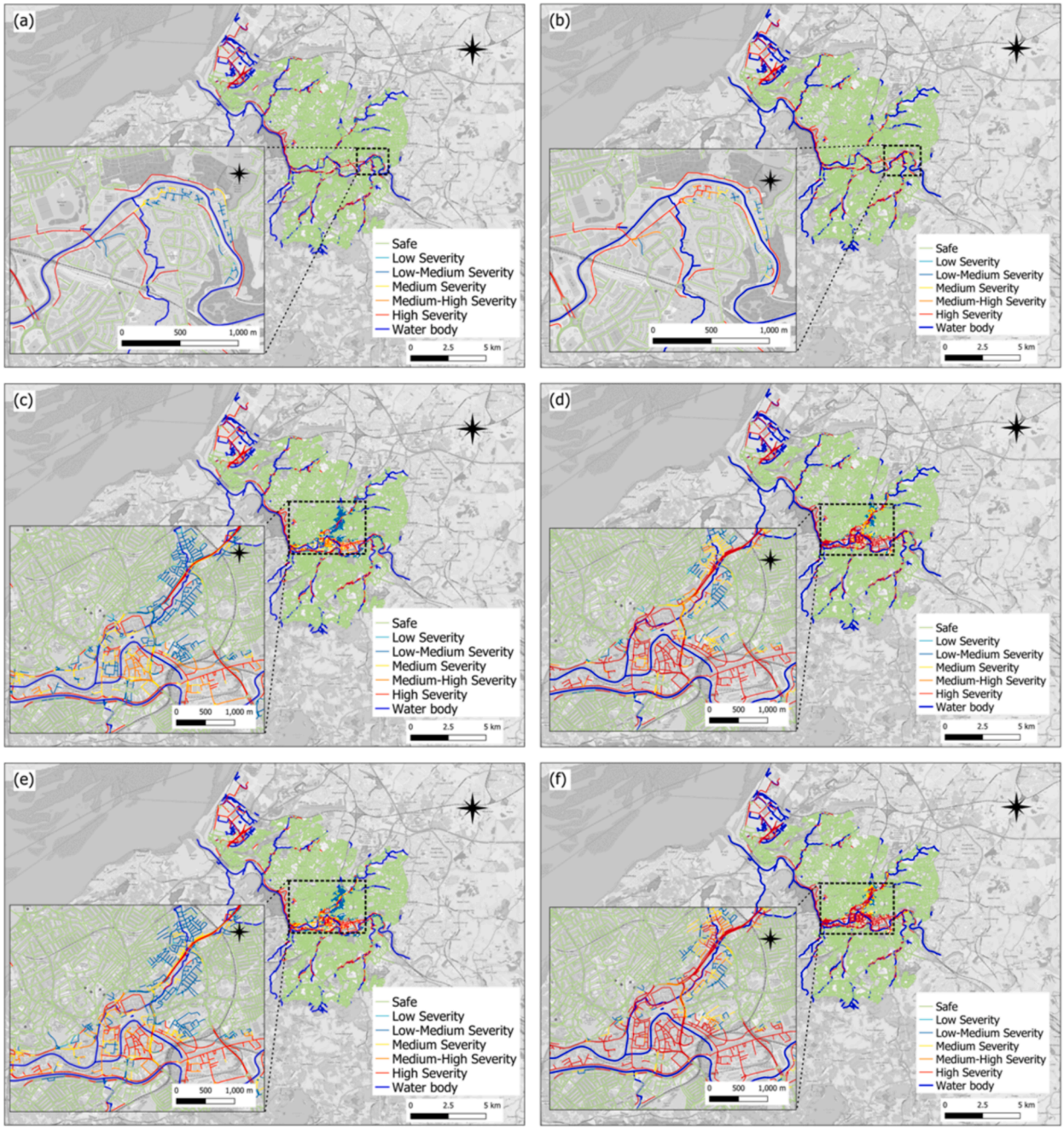

Fig. 4. Road network of Bristol flood severity mapping for SUVs and cars. (a) 100-year of SUVs; (b) 100-year of cars; (c) 200-year of SUVs; (d) 200-year of cars; (e) 500-year of SUVs; (f) 500-year of cars.

velocity is not always considered a critical intensity measure in flood risk studies. In such a lack of data, the shallow water equation is used to conservatively estimate flood velocity using flood depth when flood velocity is not available but is a necessary condition for studying flood hazard. (i.e., $u = (gh)^{0.5}$).

For the topological data of the road network, this study utilises open-source geospatial data provided by OpenStreetMap (OSM). Although OpenStreetMap (OSM) provides a rich foundation of open-source geographic information data, its decentralised nature and reliance on volunteer contributions can lead to data heterogeneity and incompleteness (Jokar Arsanjani et al., 2015). To address the limitations such as heterogeneity and incompleteness of OSM road network data, OSM data was manually revised based on Google Maps. The graph-based road network components are described in detail, such as geometry and design speed. More attributes can be added if needed (Muhammad et al., 2021).

Finally, isochrones are computed using critical facilities in Bristol, such as hospitals and fire brigade stations. This paper focuses on the Bristol Royal Infirmary (BRI) hospital, which is located in the city centre and is essential during emergencies (Fig. 3).

4. Results

4.1. Links severity factors

In this section, the results of the methodology explained in Section 2 are presented. The Severity Factors are computed for two vehicle typologies (i.e., SUVs and cars) and the ten return periods presented in Section 3.

Fig. 4 shows the main results. For T_R lower than 100 years, the severity factor is generally low and similar for both vehicle typologies (Fig. 4a and 4b). Only the roads along the rivers Avon and Frome exhibit High severity (see Supplementary Material A Figure S1 for more details). For T_R larger than 100 years, the severity of the road network links in the city centre changes drastically for both SUVs and cars. This phenomenon may be attributed to the relatively low elevation of Bristol city centre. For a return period of 200 years, several roads reach "High" severity for cars (Fig. 4d) but not SUVs (Fig. 4c). Only for a 500-years return period is it possible to observe severity "Medium" to "High" for SUVs (Fig. 4e); for such a return period, the severity for cars is always "High" for the flooded links. For extreme flood events (i.e., $T_R = 1000$ years), most of the flooded links become "High" severity regardless of whether SUVs or cars are considered. All the results are also presented in the Supplementary Material A Figure S1.

Fig. 5 shows the trends of the severity factors for all return periods for SUVs (Fig. 5a) and cars (Fig. 5b), respectively. This paper shows the trend of each severity level (excluding "Safe") as a percentage of the total number of roads. When the curve experiences a decrease in value, it indicates a transition of severity from one level to another. Also, Table 3 shows the proportion of "High" severity roads among all flood-affected roads. Analysing the count of "High" severity cases for SUVs and cars reveals that with an increase in flood return period, cars exhibit a notably higher frequency of "High" severity classification than SUVs.

Under increasing T_R, severity level trends for SUVs and cars present an upward trend with distinct patterns. When T_R equals 200 years, the growth trends of "Low-Medium" severity exceeded the growth trend of "High" severity. The orange line is growing faster than the green line (Fig. 5a). Many roads along Frome and around Avon are experiencing "Low-Medium" severity during the 200-year flood return period. Although the number of "High" severity roads is also increasing, only a few appear near water bodies (Fig. 4c). When T_R is equal to 200 years, the flood intensity increases, resulting in a greater number of roads being affected by flooding. However, among the roadways affected by flooding, a higher proportion still maintain functionality, allowing vehicular passage. Therefore, while the number of "High" severity roads is increasing, their percentage remains lower than that of "Low-Medium" severity roads. Although other severity levels increased for cars, the growth of "High" severity dominated.

When T_R is larger than 200 years, the proportion of "Low" severity, "Low-Medium" severity, "Medium" severity, and "Medium-High" severity to the total number of roads has basically not increased, and only "High" severity has increased significantly (Fig. 5b). This observation implies that, for the same T_R, cars are more susceptible to the floods. Therefore, for the city of Bristol, most of the road

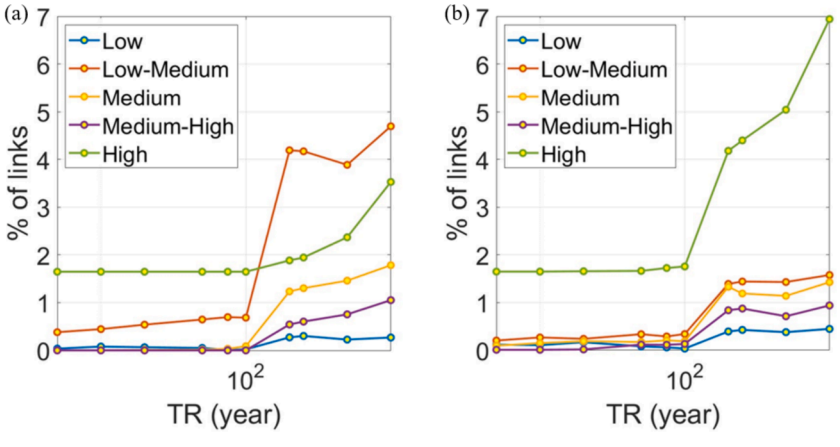

Fig. 5. Severity Factor percentages out of the total number of roads for (a) SUVs and (b) cars.

Table 3
Number of roads of each severity level and the percentage of High Severity of all flood-affected roads.

T_R	Flood-affected roads	High severity roads	% of High severity out of Flood-affected roads	Flood-affected roads	High severity roads	% of High severity out of Flood-affected roads
	SUVs			cars		
5	575	459	79.8 %	575	459	79.8 %
10	605	459	75.9 %	605	459	75.9 %
20	629	459	72.9 %	629	461	73.0 %
50	657	459	69.9 %	657	463	70.5 %
75	664	459	69.1 %	664	480	72.3 %
100	680	459	67.5 %	680	489	72.0 %
200	2264	525	23.2 %	2264	1165	51.4 %
250	2319	542	23.4 %	2319	1126	52.9 %
500	2423	660	27.2 %	2423	1405	58.0 %
1000	3156	983	31.1 %	3156	1935	61.3 %

networks lose functionality for cars for return periods larger or equal to 200 years. Under the same high-intensity flood disasters (T_R 200 years and greater), most flood-affected roads remain open to SUVs. This result suggests that for SUVs, the road network of Bristol exhibits greater functionality to flood hazards.

4.2. Road network functionality analysis

The severity level of a road determines its level of functionality. From "Safe" to "High" severity, the maximum allowable vehicle speed gradually decreases from the free-flow maximum speed limit to 0 (where 0 indicates a complete loss of road functionality). When

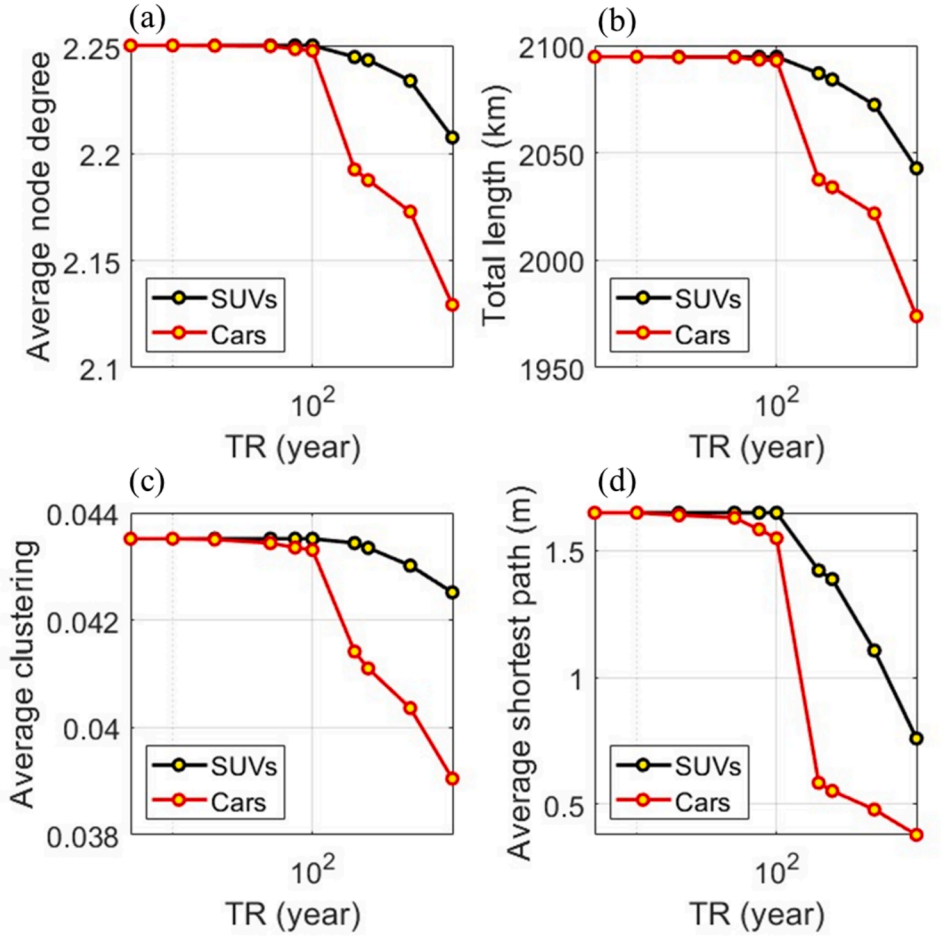

Fig. 6. Road network functionality analysis of SUVs and cars. (a) average node degree; (b) total length; (c) average clustering; (d) average shortest path.

the severity of the road is classified as "High" severity, it indicates that the road is closed (i.e., non-functional). In the graph of the road network, roads that have become non-functional will be removed. As a result, the overall functionality of the road network will decline. As described in Section 2.4, the assessment of the overall road network functionality is based on four metrics: average node degree, average shortest path, average clustering, and total accessible length (see Table 2).

Fig. 6 illustrates the variations in the four metrics of the entire road networks for SUVs and cars across different flood return periods. When a 200-year T_R, average node degree, average clustering, average shortest path, and total length all experienced obvious declines regardless of whether SUVs or cars are considered. This phenomenon indicates that road network functionality decreases significantly for SUVs and cars when the flood return periods are equal or larger than 200 years. As a result, the connectivity of the road network is reduced, and vehicles need to be rerouted from origin to destination and travel longer distances.

The extent of functionality variation in average node degree, average clustering, average shortest path, and total length differs across diverse vehicle types. When T_R is equal or larger than 200 years, the rate of decay in the four metrics of functionality for cars exceeds that of SUVs. This result shows that more roads are closed to cars than to SUVs. Under high-intensity flood events ($T_R \geq 200$ years), the connectivity, redundancy, and robustness of the road network are more vulnerable to cars. In the event of a high-intensity flood, it becomes essential to strengthen the overall resilience of the road network by implementing interventions that prioritise the

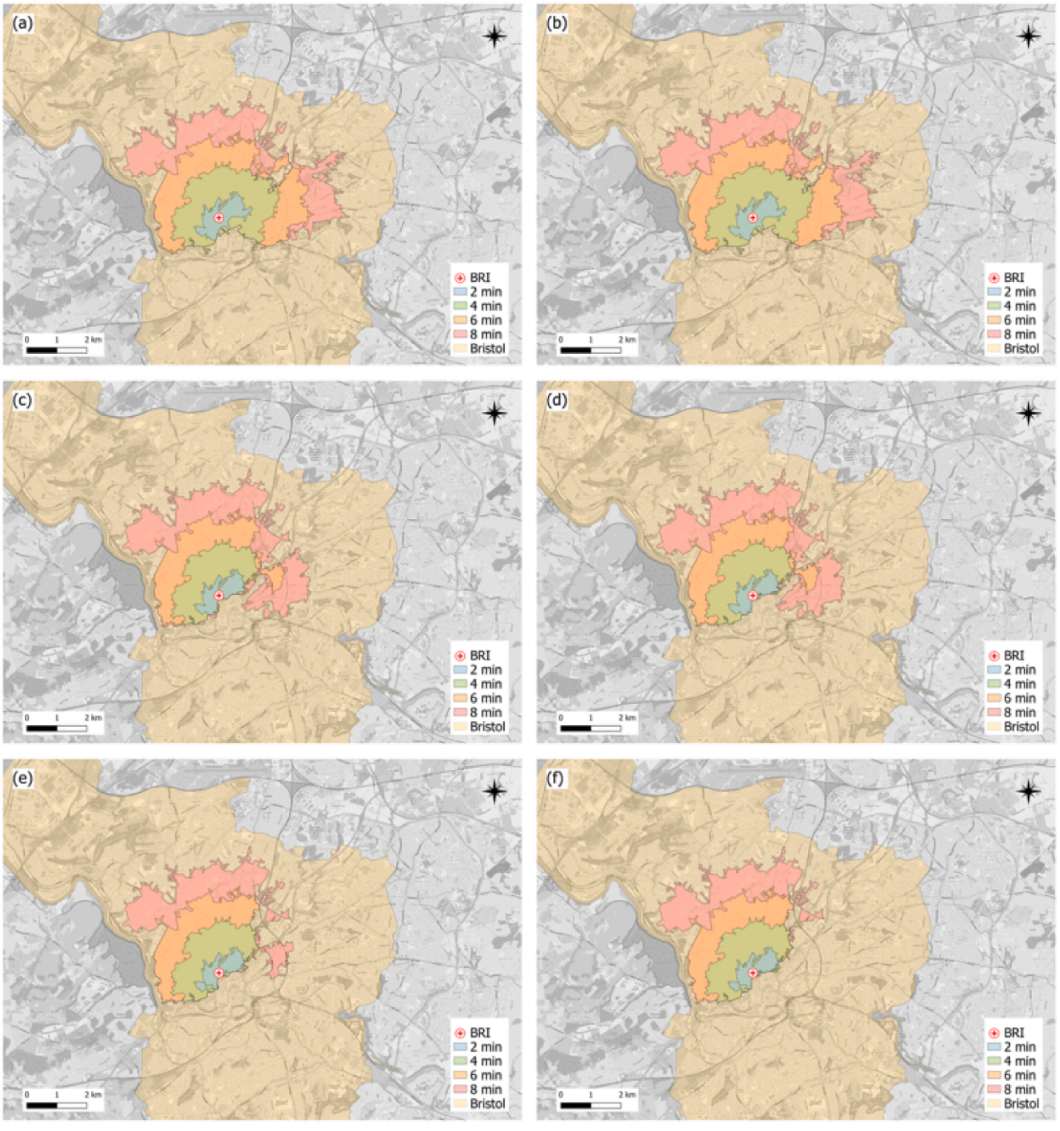

Fig. 7. Time-based isochrone of SUVs and cars from Bristol Royal Infirmary. (a) 100-year flood return period time-based isochrone of SUVs; (b) 100-year flood return period time-based isochrone of cars; (c) 200-year flood return period time-based isochrone of SUVs; (d) 200-year flood return period time-based isochrone of cars; (e) 500-year flood return period time-based isochrone of SUVs; (f) 500-year flood return period time-based isochrone of cars.

enhancement of the road functionality for cars (e.g. improving drainage).

4.3. Time-based isochrone analysis

"High" severity roads have lost their functionality, becoming closed to vehicles. For roads categorised as "Low" severity, "Low-Medium" severity, "Medium" severity, and "Medium-High" severity in the flood hazards, although they remain accessible to vehicles, drivers must reduce their travel speeds to ensure a safe journey. Consequently, when roads are affected by flood hazards, the travel time for vehicles from the same origin to the same destination is increased, thereby diminishing the efficiency of the road network. This paper applies time-based isochrones centred around hospitals to investigate further the road network's functionality under varying flood return periods. This study assumes perfect driver behaviour, implying that all drivers know the road's inundation conditions. Also, the isochrones presented in this paper reflect the inherent traffic performance of the road network under flood inundation, representing a static ideal scenario that disregards real-world driver behaviour and congestion. In particular, the Bristol Royal Infirmary is selected as this study's focal point of investigation.

According to the British new ambulance standard, ambulances must reach patients' locations within an 8-minute timeframe (Coles et al., 2017; Green et al., 2017; CHANGE, 2022). This study considers four time-based isochrones based on this standard (2, 4, 6, and 8 min) to show more details about the reachability and efficiency for emergency response.

Fig. 7 displays time-based isochrone maps for both SUVs and cars for 100-year, 200-year, and 500-year return periods (more results are provided in the supplementary material B Figure S2). For the 100-year flood return period scenario (Fig. 7a and 7b), no significant distinction is observed between the time-based isochrone areas reachable from Bristol Royal Infirmary for SUVs and cars. As per the analysis in Section 4.1, the road network exhibits nearly identical functionality for SUVs and cars for T_R 100-year scenarios.

For the 200-year flood return period (Fig. 7c and 7d), SUVs and cars travelling eastward from Bristol Royal Infirmary experience a performance reduction. Specifically, for SUVs, a portion of the area reachable within 4 min from Bristol Royal Infirmary now requires 8 min for access. Moreover, the area to the southeast of the BRI that can be reached within 6 min by SUVs is significantly reduced. For cars and for the 200-year flood return period, the 4-min accessible area in the southeast direction of the BRI becomes 8 min. Compared to SUVs, the area south of the BRI, previously reachable by car within 8 min, has completely disappeared.

With a 500-year flood return period, Fig. 7e and Fig. 7f show that the accessibility of the southeastern area of BRI becomes more

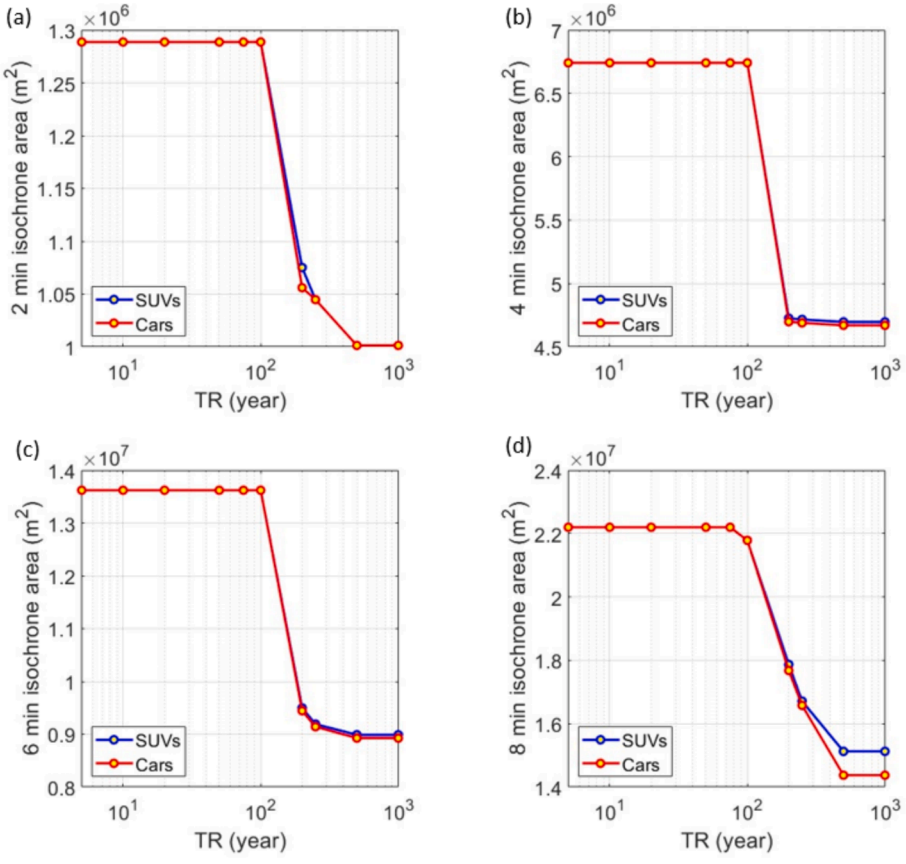

Fig. 8. Isochrone areas of different time windows based on the origin location Bristol Royal Infirmary; a) 2-min time window; b) 4-min time window; c) 6-min time window; d) 8-min time window.

limited and unreachable. Specifically, for SUVs, areas previously reachable within 6 min from Bristol Royal Infirmary are no longer accessible. Meanwhile, the 8-min isochrone area is further reduced. For cars, when T_R equals 500 years, the 6-min and 8-min isochrone areas further shrink, and the southeastern area of the BRI becomes completely inaccessible. These findings demonstrate a substantial decrease in travel efficiency along the roads eastward from Bristol Royal Infirmary when subjected to flooding. Therefore, for flood risk management, it is necessary to implement intervention to enhance the accessibility and travel efficiency of the roads eastward from Bristol Royal Infirmary.

Fig. 8 illustrates how the area covered by the isochrones varies with the return period. For flood scenarios with return periods equal to or less than 100 years, there is no difference in the isochrone areas between SUVs and cars at 2, 4, 6 and 8 min. For the 200-year flood return period, a significant reduction is observed in all isochrone areas. Within the 2-min isochrone zone, the reachable area of SUVs is larger than that of cars only at the 200-year flood scenario (Fig. 8a). This result suggests that in the vicinity of Bristol Royal Infirmary, some roads have higher severity for cars than SUVs.

In the 4-, 6- and 8-min isochrone zones, when flood return periods equal or exceed 200 years, the reachable area for SUVs is larger than that computed for cars (Fig. 8b, 8c, and 8d). Especially for the 8-min isochrone zone, the reachable area for SUVs is much larger than that of cars (Fig. 8d). This result indicates that during high-intensity floods ($T_R \geq 200$ years), road accessibility for cars is significantly constrained farther away from the Bristol Royal Infirmary. As depicted in Fig. 7f, it is evident that during a 500-year return period flood, all areas to the southeast of BRI become inaccessible to cars. Therefore, this finding suggests that during a flood event, emergency ambulance traffic efficiency originating from BRI may be markedly reduced in the southeastern direction of the Bristol Royal Infirmary.

The results indicate a lack of connectivity redundancy around the BRI. Additionally, the road near the vehicle entrance and exit in the southeast direction has a low-lying elevation, making it prone to surface runoff accumulation, obstructing accessibility from the southeast direction. The selection of BRI as the starting point reflects the limitations of road accessibility following flooding; however, accessibility outcomes may differ significantly for different critical amenities.

5. Discussion and future research

The significance of this study regards three aspects. Firstly, this study defines a methodological contribution to the state-of-the-art transportation infrastructure assessment by integrating the impact of two key flood attributes (flood depth and flood velocity). Such an approach offers a more comprehensive framework for understanding flood-related road network risks. This study also fills the gaps left by previous literature, which only focuses on either flood depth-related (Choo et al., 2020; Alabbad et al., 2021; Shahdani et al., 2022) or flood velocity-related (Xia et al., 2011a; Wang et al., 2021) risk to road network individually. It is noteworthy that the methodology presented in this study is not limited to fluvial and pluvial flooding but can be extended to a wider range of inundation scenarios, including tidal inundation and tsunamis.

Secondly, this research investigates the severity of various vehicle types when handling different intensities of flood events. This analysis explains how roads affected by floods respond differently for various types of vehicles. This approach is essential for analysing the impact on traffic flow changes and traffic congestion conditions following the complete or partial loss of functionality in the link in the future.

Lastly, a contribution lies in establishing time-based isochrone maps originating from hospital locations, accounting for varying road conditions during flood events. This approach offers an initial strategy for emergency response efforts, aiding in efficiently deploying resources and improving overall preparedness and response within the road network. Consequently, this study provides valuable insights into the functionality assessment of road networks by amalgamating flood roadworthiness and graph topology considerations.

However, it is important to acknowledge the presence of certain limitations. First, this study does not investigate all uncertainties affecting road network functionality. This limitation is because, for example, there is a lack of probabilistic models for the adopted vehicle vulnerability model. Second, this study is limited in scope as it exclusively focuses on assessing the flood severity impacts on SUVs and cars. The classification of vehicle types is relatively coarse, and the sample size remains constrained, potentially overlooking the nuances of other vehicle categories. Third, in analysing traffic within road networks of varying severity levels, the study assumes that all vehicles travel at their maximum safe speeds without accounting for real-world factors such as traffic signals and actual traffic flow. As a result, the analysis of time-based isochrones exhibits an idealised representation. Fourthly, this study focuses on analysing static flood scenarios with maximum inundation depth, consistently with the adopted simulated static road network topology performance. Analogously, any agent-based approach for traffic simulation, for consistency, should be coupled with a dynamic flood model (e.g. Muhammad et al. 2024). In addition, the flood velocity used in this paper is based on a conservative simulation of the flood depth and does not represent the actual flood velocity. However, more sophisticated flood hazard models can provide more realistic flood velocity values. Finally, a constant flood return periods in space was assumed in this study. To expand the analysis to large scale, realistic event footprints from a stochastic flood model could be used to handle the spatial variability in return periods seen for actual floods (Bates et al., 2023).

Future research must explore road network functionality loss during flooding in a probabilistic manner. However, such a probabilistic approach requires the availability of rigorous and reliable deterministic mechanistic models that can be used to propagate the uncertainties and that are the focus of this paper; in other words, this paper provides an accessible means to assess vulnerability. The inherent uncertainty tackled in this study stems from the hazard assessment that depends on precipitations, humidity conditions, surface roughness, and antecedent moisture conditions, to mention a few. Considering multiple return periods shows the key interest in the main temporal uncertainty associated with rain intensity. Furthermore, future research can consider vehicle travel speeds on roads

to encompass the mutual influence among vehicles and the waiting times at traffic signals. Moreover, due to the high dynamicity and uncertainty of traffic, future research must simulate driver behaviours under different scenarios, such as choosing the shortest travel time path, the shortest travel distance path, or a combination of both. This approach aims to align traffic flow distribution and variation more closely with real-world conditions, thereby more accurately identifying roads prone to congestion.

6. Conclusion

This study presents an innovative approach by integrating the effects of flood depth and flow velocity on the stability of different vehicle types (i.e., SUVs and cars) and categorising road severity within the road network of Bristol during floods. The research assesses how the functionality of the road network of Bristol for SUVs and cars varies with different flood return periods based on severity levels. Furthermore, it investigates changes in time-based accessibility from Bristol Royal Infirmary as origin/destination. The following three points can summarise the key findings of this study:

- Small vehicles (cars) exhibit significantly lower flooding resistance than larger vehicles (SUVs). Therefore, for emergency rescue vehicles, using SUV-like vehicles rather than traditional cars is recommended to study roadworthiness during floods in the lack of more specific models.
- During a 200-year flood return period, the functionality of the road network experiences a notable decline for both SUVs and cars; for cars mainly, the road network shows a particularly dramatic decrease in functionality.
- The area accessible to SUVs to the southeast of Bristol Royal Infirmary is considerably reduced when flood return periods equal to or exceed 200 years; furthermore, under extreme flood events (i.e., a return period of 500 years), the accessibility of cars in the southeastern direction of Bristol Royal Infirmary becomes impossible.

These observations underscore the critical importance of considering vehicle type and flood return periods when assessing the impact of flooding on road network functionality. The findings of this study offer critical insights for future research aimed at enhancing the resilience of road networks during flood events. Specifically, it identifies key information regarding flood return periods associated with significant declines in road network functionality and vulnerable road network locations within the Bristol area.

In future research, the integration of traffic flow variations within the road network across various flood return period scenarios should be pursued. Additionally, an investigation into the betweenness centrality of the road network should be conducted, leveraging vehicle travel speeds to elucidate the critical roads within the road network of Bristol. These efforts will serve as a foundation for informing the development of flood response intervention measures in the future.

CRediT authorship contribution statement

Ke He: Writing – review & editing, Writing – original draft, Visualization, Software, Methodology, Formal analysis, Data curation, Conceptualization. **Maria Pregnolato:** Writing – review & editing, Supervision. **Neil Carhart:** Writing – review & editing, Supervision. **Jeffrey Neal:** Writing – review & editing, Resources. **Raffaele De Risi:** Writing – review & editing, Visualization, Supervision, Software, Methodology, Conceptualization.

Declaration of competing interest

The authors declare that they have no known competing financial interests or personal relationships that could have appeared to influence the work reported in this paper.

Acknowledgements

Flood data is provided by the flood hazard company Fathom, Bristol. Raffaele De Risi acknowledges the project Community and Infrastructure Resilience to Climate-geological Long-term Effects (CIRCLE), ES/Z000122/1.

Appendix A. Supplementary data

Supplementary data to this article can be found online at https://doi.org/10.1016/j.trd.2024.104354.

References

Abdulla, B., Kiaghadi, A., Rifai, H.S., Birgisson, B., 2020. Characterisation of vulnerability of road networks to fluvial flooding using SIS network diffusion model. J. Infrastruct. Preserv. Resilience 1 (1). https://doi.org/10.1186/s43065-020-00004-z.

Alabbad, Y., Mount, J., Campbell, A.M., Demir, I., 2021. Assessment of transportation system disruption and accessibility to critical amenities during flooding: Iowa case study. Sci. Total Environ. 793, 148476 https://doi.org/10.1016/j.scitotenv.2021.148476.

Argyroudis, S.A., Mitoulis, S.A., Hofer, L., Zanini, M.A., Tubaldi, E., Frangopol, D.M., 2020. Resilience Assessment Framework for Critical Infrastructure in a multi-hazard environment: Case study on transport assets. Sci. Total Environ. 714, 136854 https://doi.org/10.1016/j.scitotenv.2020.136854.

Arrighi, C., Alcèrreca-Huerta, J.C., Oumeraci, H., Castelli, F., 2015. Drag and lift contribution to the incipient motion of partly submerged flooded vehicles. J. Fluids Struct. 57, 170–184. https://doi.org/10.1016/j.jfluidstructs.2015.06.010.

ARUP, 2020. *Bristol Avon Flood Strategy*. tech. Bristol City Council. Available at: https://democracy.bristol.gov.uk/documents/s57930/Appendix%20A%20Strategic%20Outline%20Case.pdf.

Bainbridge, L., 2021, November 13. What is an isochrone map? A definition &; examples. *TravelTime*. October 31, 2023, https://traveltime.com/blog/what-is-an-isochrone.

Balijepalli, C., Oppong, O., 2014. Measuring vulnerability of road network considering the extent of serviceability of Critical Road Links in urban areas. J. Transp. Geogr. 39, 145–155. https://doi.org/10.1016/j.jtrangeo.2014.06.025.

Barthélemy, J., Carletti, T., 2017. An adaptive agent-based approach to traffic simulation. Transport. Res. Proc. 25, 1238–1248. https://doi.org/10.1016/j.trpro.2017.05.142.

Bates, P.D., Savage, J., Wing, O., Quinn, N., Sampson, C., Neal, J., Smith, A., 2023. A climate-conditioned catastrophe risk model for UK flooding. Nat. Hazards Earth Syst. Sci. 23 (2), 891–908. https://doi.org/10.5194/nhess-23-891-2023.

Bocanegra, R.A., Francés, F., 2021. Assessing the risk of vehicle instability due to flooding. J. Flood Risk Manage. 14 (4) https://doi.org/10.1111/jfr3.12738.

Boeing, G., 2017. OSMnx: A python package to work with graph-theoretic OpenStreetMap Street Networks. J. Open Source Software 2 (12), 215. https://doi.org/10.21105/joss.00215.

Boeing, G., 2017. OSMNX: New methods for acquiring, constructing, analysing, and Visualising Complex Street Networks. Comput. Environ. Urban Syst. 65, 126–139. https://doi.org/10.1016/j.compenvurbsys.2017.05.004.

Bruneau, M., Chang, S., Eguchi, R., Lee, G., O'Rourke, T., Reinhorn, A., et al., 2003. A framework to quantitatively assess and enhance the seismic resilience of communities. Earthq. Spectra 19 (4), 733–752. https://doi.org/10.1193/1.1623497.

Casali, Y., Heinimann, H.R., 2019. A topological characterisation of flooding impacts on the Zurich Road Network. PLoS One 14 (7). https://doi.org/10.1371/journal.pone.0220338.

CHANGE, 2022. The New Ambulance Standards [PDF], pp. 1-5. Retrieved 2 September 2023, from https://www.england.nhs.uk/wp-content/uploads/2017/07/new-ambulance-standards-easy-read.pdf.

Choo, K.-S., Kang, D.-H., Kim, B.-S., 2020. Impact assessment of urban flood on traffic disruption using rainfall–depth–vehicle speed relationship. Water 12 (4), 926. https://doi.org/10.3390/w12040926.

Cimellaro, G.P., Reinhorn, A.M., Bruneau, M., 2010. Framework for analytical quantification of Disaster Resilience. Eng. Struct. 32 (11), 3639–3649. https://doi.org/10.1016/j.engstruct.2010.08.008.

Cimellaro, G.P., Renschler, C., Arendt, L., Bruneau, M., Reinhorn, A.M., 2011. Community resilience index for road network system. In: In *8Th International Conference on Structural Dynamics*. EURODYN, Leuven, pp. 370–376.

Coles, D., Yu, D., Wilby, R.L., Green, D., Herring, Z., 2017. Beyond 'flood hotspots': Modelling emergency service accessibility during flooding in York, UK. J. Hydrol. 546, 419–436. https://doi.org/10.1016/j.jhydrol.2016.12.013.

Costa Fonte, C., Fritz, S., Olteanu-Raimond, A., Antoniou, V., Foody, G., Mooney, P., See, L., 2017. Mapping and the Citizen Sensor. Ubiquity Press, London.

Cumbria County Council, 2010. Cumbria floods November 2009: an impact assessment. http://www.cumbria.gov.uk/eLibrary/Content/Internet/536/671/4674/4026717419.pdf last access: August 2023.

De Risi, R., Jalayer, F., De Paola, F., 2015. Meso-scale hazard zoning of potentially flood prone areas. J. Hydrol. 527, 316–325. https://doi.org/10.1016/j.jhydrol.2015.04.070.

De Risi, R., Jalayer, F., De Paola, F., Lindley, S., 2018. Delineation of flooding risk hotspots based on digital elevation model, calculated and historical flooding extents: The case of ouagadougou. Stoch. Env. Res. Risk A. 32 (6), 1545–1559. https://doi.org/10.1007/s00477-017-1450-8.

De Risi, R., Jalayer, F., De Paola, F., Carozza, S., Yonas, N., Giugni, M., Gasparini, P., 2020. From flood risk mapping toward reducing vulnerability: The case of Addis Ababa. Nat. Hazards 100 (1), 387–415. https://doi.org/10.1007/s11069-019-03817-8.

Der Kiureghian, A., 2022. Structural and system reliability. Cambridge University Press.

Do, M., Jung, H., 2018. Enhancing road network resilience by considering the performance loss and asset value. Sustainability 10 (11), 4188. https://doi.org/10.3390/su10114188.

Dong, B., Xia, J., Li, Q., Zhou, M., 2022. Risk assessment for people and vehicles in an extreme urban flood: Case study of the "7.20" flood event in Zhengzhou, China. Int. J. Disaster Risk Reduction 80, 103205. https://doi.org/10.1016/j.ijdrr.2022.103205.

El Rashidy, R.A., Grant-Muller, S., 2019. A composite resilience index for Road Transport Networks. Proc. Inst. Civ. Eng. - Transport 172 (3), 174–183. https://doi.org/10.1680/jtran.16.00139.

Evans, B., Chen, A.S., Djordjević, S., Webber, J., Gómez, A.G., Stevens, J., 2020. Investigating the effects of pluvial flooding and climate change on traffic flows in Barcelona and Bristol. Sustainability 12 (6), 2330. https://doi.org/10.3390/su12062330.

Fathom, 2023 *Home, Fathom*. Available at: https://www.fathom.global/ (accessed: August 8, 2023).

Gauthier, P., Furno, A., El Faouzi, N.-E., 2018. Road network resilience: How to identify critical links subject to day-to-day disruptions. Transport. Res. Record: J. Transport. Res. Board 2672 (1), 54–65. https://doi.org/10.1177/0361198118792115.

Green, D., Yu, D., Pattison, I., Wilby, R., Bosher, L., Patel, R., Thompson, P., Trowell, K., Draycon, J., Halse, M., Yang, L., Ryley, T., 2017. City-scale accessibility of emergency responders operating during flood events. Nat. Hazards Earth Syst. Sci. 17 (1), 1–16. https://doi.org/10.5194/nhess-17-1-2017.

Hawker, L., Uhe, P., Paulo, L., Sosa, J., Savage, J., Sampson, C., Neal, J., 2022. A 30 m global map of elevation with forests and buildings removed. Environ. Res. Lett. 17 (2), 024016 https://doi.org/10.1088/1748-9326/ac4d4f.

He, K., Risi, R.D., Pregnolato, M., Carhart, N., Neal, J., 2023. Graph-based Framework for Road Network Performance and Flood Risk Assessment. In: *14th International Conference on Applications of Statistics and Probability in Civil Engineering*. Dublin; ICASP14, pp. 1–7.

Henry, E., Furno, A., Faouzi, N., 2021. A Graph-based Approach with Simulated Traffic Dynamics for the Analysis of Transportation Resilience in Smart Cities. Presentation, Washington, D.C.

Hooper, E., Chapman, L., Quinn, A., 2012. Investigating the impact of precipitation on vehicle speeds on UK motorways. Meteorol. Appl. 21 (2), 194–201. https://doi.org/10.1002/met.1348.

Jalayer, F., De Risi, R., De Paola, F., Giugni, M., Manfredi, G., Gasparini, P., Topa, M.E., Yonas, N., Yeshitela, K., Nebebe, A., Cavan, G., Lindley, S., Printz, A., Renner, F., 2014. Probabilistic GIS-based method for delineation of urban flooding risk hotspots. Nat. Hazards 73, 975–1001. https://doi.org/10.1007/s11069-014-1119-2.

Jokar Arsanjani, J., Zipf, A., Mooney, P., Helbich, M., 2015. An introduction to OpenStreetMap in Geographic Information Science: Experiences, research, and applications. OpenStreetMap in GIScience: Experiences, research, and applications, 1-15.

Kalantari, Z., Cavalli, M., Cantone, C., Crema, S., Destouni, G., 2017. Flood probability quantification for road infrastructure: Data-driven spatial-statistical approach and case study applications. Sci. Total Environ. 581–582, 386–398. https://doi.org/10.1016/j.scitotenv.2016.12.147.

Karduni, A., Kermanshah, A., Derrible, S., 2016. A protocol to convert spatial polyline data to network formats and applications to World Urban Road Networks. Sci. Data 3 (1). https://doi.org/10.1038/sdata.2016.46.

Kim, S., Seyedi, M., Kim, H.-K., 2022. Risk assessment of wind-induced vehicle accidents on long-span bridges using onsite wind and Traffic Data. J. Struct. Eng. 148 (10) https://doi.org/10.1061/(asce)st.1943-541x.0003455.

Kim, S.-J., Yoo, C.-H., Kim, H.-K., 2016. Vulnerability assessment for the hazards of crosswinds when vehicles cross a bridge deck. J. Wind Eng. Ind. Aerodyn. 156, 62–71. https://doi.org/10.1016/j.jweia.2016.07.005.

Kim, S.-J., Shim, J.-H., Kim, H.-K., 2020. How wind affects vehicles crossing a double-deck suspension bridge. J. Wind Eng. Ind. Aerodyn. 206, 104329 https://doi.org/10.1016/j.jweia.2020.104329.

Kramer, M., Terheiden, K., Wieprecht, S., 2016. Safety criteria for the trafficability of inundated roads in urban floodings. Int. J. Disaster Risk Reduct. 17, 77–84. https://doi.org/10.1016/j.ijdrr.2016.04.003.

Lazzarin, T., Viero, D.P., Molinari, D., Ballio, F., Defina, A., 2022. Flood damage functions based on a single physics- and data-based impact parameter that jointly accounts for water depth and velocity. J. Hydrol. 607, 127485 https://doi.org/10.1016/j.jhydrol.2022.127485.

Lopez, P.A., Behrisch, M., Bieker-Walz, L., Erdmann, J., Flötteröd, Y., Hilbrich, R., Lücken, L., Rummel, J., Wagner, P., Wiessner, E., 2018. Microscopic traffic simulation using SUMO. IEEE Xplore. https://doi.org/10.1109/ITSC.2018.8569938.

Martínez-Gomariz, E., Gómez, M., Russo, B., Djordjević, S., 2017. A new experiments-based methodology to define the stability threshold for any vehicle exposed to flooding. Urban Water J. 14 (9), 930–939. https://doi.org/10.1080/1573062x.2017.1301501.

McCarthy, S., Magramo, K., 2023. More than a million displaced and dozens dead after record rain drenches northeastern China. CNN. https://www.cnn.com/2023/08/04/china/china-northeast-hebei-beijing-flooding-recovery-intl-hnk/index.html.

Merschman, E., Doustmohammadi, M., Salman, A., Anderson, M., 2020. Postdisaster decision framework for bridge repair prioritization to improve road network resilience. Transport. Res. Record: J. Transport. Res. Board 2674 (3), 81–92. https://doi.org/10.1177/0361198120908870.

Muhammad, A., De Risi, R., De Luca, F., Mori, N., Yasuda, T., Goda, K., 2021. Are current tsunami evacuation approaches safe enough? Stoch. Env. Res. Risk A. https://doi.org/10.1007/s00477-021-02000-5 \.

Muhammad, A., De Risi, R., De Luca, F., Kongko, W., Mori, N., Yasuda, T., Goda, K., 2024. Integrated tsunami risk framework considering agent-based evacuation modelling: The case of Saga, Kochi Prefecture, Japan. Int. J. Disaster Risk Reduct. 101, 104193 https://doi.org/10.1016/j.ijdrr.2023.104193.

Mukherjee, S., 2012. Statistical analysis of the road network of India. Pramana 79 (3), 483–491. https://doi.org/10.1007/s12043-012-0336-z.

Nelson, A., Lindbergh, S., Stephenson, L., Halpern, J., Arroyo, F.A., Espinet, X., González, M.C., 2019. Coupling natural hazard estimates with road network analysis to assess vulnerability and risk: Case study of Freetown (Sierra Leone). Transport. Res. Record: J. Transport. Res. Board 2673 (8), 11–24. https://doi.org/10.1177/0361198118822272.

Nelson, A., By, R., Thomas, T., Girgin, S., Brussel, M., Venus, V., Ohuru, R., 2021. The resilience of domestic transport networks in the context of food security – A multi-country analysis: Background Paper for the State of Food and Agriculture. Food & Agriculture Org 52.

NetworkX, 2022. *NetworkX — NetworkX documentation*. Networkx.org. Retrieved 15 August 2023, from https://networkx.org/.

Ogie, R.I., Holderness, T., Dunn, S., Turpin, E., 2018. Assessing the vulnerability of hydrological infrastructure to flood damage in coastal cities of developing nations. Comput. Environ. Urban Syst. 68, 97–109. https://doi.org/10.1016/j.compenvurbsys.2017.11.004.

Otković, I.I., Deluka-Tibljaš, A., Šurdonja, S., 2020. Validation of the calibration methodology of the micro-simulation traffic model. Transp. Res. Procedia 45, 684–691. https://doi.org/10.1016/j.trpro.2020.02.110.

Panakkal, P., Wyderka, A.M., Padgett, J.E., Bedient, P.B., 2023. Safer this way: Identifying flooded roads for facilitating mobility during floods. J. Hydrol. 625, 130100 https://doi.org/10.1016/j.jhydrol.2023.130100.

Podobnikar, T., 2009. Methods for visual quality assessment of a digital terrain model. *S.A.P.I.EN*, 2.2(2). https://journals.openedition.org/sapiens/738#article-738.

Pregnolato, M., Ford, A., Robson, C., Glenis, V., Barr, S., Dawson, R., 2016. Assessing urban strategies for reducing the impacts of extreme weather on Infrastructure Networks. R. Soc. Open Sci. 3 (5), 160023 https://doi.org/10.1098/rsos.160023.

Pregnolato, M., Ford, A., Wilkinson, S.M., Dawson, R.J., 2017. The impact of flooding on road transport: A depth-disruption function. Transp. Res. Part D: Transp. Environ. 55, 67–81. https://doi.org/10.1016/j.trd.2017.06.020.

Pyatkova, K., Chen, A.S., Djordjević, S., Butler, D., Vojinović, Z., Abebe, Y.A., Hammond, M., 2018. Flood impacts on road transportation using microscopic traffic modelling techniques. Lecture Notes in Mobility 115–126. https://doi.org/10.1007/978-3-319-33616-9_8.

Shahdani, F., Santamaria-Ariza, M., Sousa, H., Coelho, M., Matos, J., 2022. Assessing flood indirect impacts on road transport networks applying mesoscopic traffic modelling: the case study of Santarém, Portugal. *Appl. Sci.* 12 (6), 3076. https://doi.org/10.3390/app12063076.

Shu, C., Xia, J., Falconer, R.A., Lin, B., 2011. Incipient velocity for partially submerged vehicles in floodwaters. J. Hydraul. Res. 49 (6), 709–717. https://doi.org/10.1080/00221686.2011.616318.

Śleszyński, P., Olszewski, P., Dybicz, T., Goch, K., Niedzielski, M.A., 2023. The ideal isochrone: Assessing the efficiency of Transport Systems. Res. Transp. Bus. Manag. 46, 100779 https://doi.org/10.1016/j.rtbm.2021.100779.

Teo, F.Y., Xia, J., Falconer, R.A., Lin, B., 2012. Experimental studies on the interaction between vehicles and floodplain flows. Int. J. River Basin Manage. 10 (2), 149–160. https://doi.org/10.1080/15715124.2012.674040.

Toda, K., Ishigaki, T., Ozaki, T., 2013. Experiments study on floating car in flooding. In: International Conference on Flood Resilience 2013 (ICFR 2013), Experiences in Asia and Europe, Exeter (UK).

Wang, N., Hou, J., Du, Y., Jing, H., Wang, T., Xia, J., Gong, J., Huang, M., 2021. A dynamic, convenient and accurate method for assessing the flood risk of people and vehicle. Sci. Total Environ. 797, 149036 https://doi.org/10.1016/j.scitotenv.2021.149036.

Wang, B., 2018. Flood immunity for a road or bridge: what benefits it can bring to road users, road authority and broad community?. In Australasian Transport Research Forum 2018 (pp. 1-2). Darwin. Retrieved 03 August 2023.

Wardhana, K., Hadipriono, F.C., 2003. Analysis of recent bridge failures in the United States. J. Perform. Constr. Facil 17 (3), 144–150. https://doi.org/10.1061/(asce)0887-3828(2003)17:3(144).

Xia, J., Falconer, R.A., Lin, B., Tan, G., 2011. Numerical assessment of flood hazard risk to people and vehicles in flash floods. Environ. Model. Softw. 26 (8), 987–998. https://doi.org/10.1016/j.envsoft.2011.02.017.

Xia, J., Teo, F.Y., Lin, B., Falconer, R.A., 2011. Formula of incipient velocity for flooded vehicles. Nat. Hazards 58 (1), 1–14. https://doi.org/10.1007/s11069-010-9639-x.

Xia, J., Falconer, R.A., Xiao, X., Wang, Y., 2014. Criterion of vehicle stability in floodwaters based on theoretical and experimental studies. Nat. Hazards 70 (2), 1619–1630. https://doi.org/10.1007/s11069-013-0889-2.

Xia, J., Teo, F.Y., Falconer, R.A., Chen, Q., Deng, S., 2016. Hydrodynamic experiments on the impacts of vehicle blockages at bridges. J. Flood Risk Manage. 11 https://doi.org/10.1111/jfr3.12228.

Yin, J., Ye, M., Yin, Z., Xu, S., 2014. A review of advances in urban flood risk analysis over China. Stoch. Env. Res. Risk A. 29 (3), 1063–1070. https://doi.org/10.1007/s00477-014-0939-7.

Yin, J., Yu, D., Yin, Z., Liu, M., He, Q., 2016. Evaluating the impact and risk of pluvial flash flood on intra-urban road network: A case study in the city center of Shanghai, China. J. Hydrol. 537, 138–145. https://doi.org/10.1016/j.jhydrol.2016.03.037.

Zhang, N., Alipour, A., 2019. Integrated Framework for risk and Resilience Assessment of the road network under inland flooding. Transport. Res. Record: J. Transport. Res. Board 2673 (12), 182–190. https://doi.org/10.1177/0361198119855975.

Zhang, Y., Li, X., Zhang, Q., 2019. Road topology refinement via a multi-conditional generative adversarial network. Sensors 19 (5), 1162. https://doi.org/10.3390/s19051162.